Appl. Phys. A 80, 675–682 (2005)
DOI: 10.1007/s00339-004-3109-9

Applied Physics A
Materials Science & Processing

J.I. PAREDES[1,2,✉]
M. BURGHARD[1]
A. MARTÍNEZ-ALONSO[2]
J.M.D. TASCÓN[2]

Graphitization of carbon nanofibers: visualizing the structural evolution on the nanometer and atomic scales by scanning tunneling microscopy

[1] Max-Planck-Institut für Festkörperforschung, Heisenbergstrasse 1, 70569 Stuttgart, Germany
[2] Instituto Nacional del Carbón, CSIC, Apartado 73, 33080 Oviedo, Spain

Received: 1 June 2004/Accepted: 21 October 2004
Published online: 15 December 2004 •

ABSTRACT The structural evolution of carbon nanofibers submitted to high-temperature (1800, 2300, and 2800 °C) heat treatments has been investigated at the nanometric and atomic scales by means of scanning tunneling microscopy (STM). To complement the local STM observations, X-ray diffraction and Raman spectroscopy characterization of the samples were also carried out. On the nanometer scale, the as-grown nanofibers displayed an isotropic platelet morphology that developed into striped arrangements of increasing width at 1800 and 2300 °C, and into large, atomically flat terraces at 2800 °C. On the atomic scale, the starting nanofibers were characterized by tiny ($\lesssim 2$ nm) crystallites. The crystallites were observed to coalesce at 1800 °C into appreciably larger (~ 3–4 nm) although still defective units. Atomic structures evidencing truly graphitic ordering (i.e. the typical STM triangular pattern with a periodicity of 0.25 nm) started to develop at 2300 °C. At this temperature, a segregation of graphitic domains and highly defective areas was noticed and attributed mainly to the mobility and subsequent aggregation of point defects (atomic vacancies). Long-range atomic-scale order was generally established in the nanofibers heat treated at 2800 °C, where only some incompletely graphitized, fragmentary graphenes were left on the surface.

PACS 81.07.-b; 81.40.Ef; 68.37.Ef

1 Introduction

Carbon nanofibers (CNFs), obtained by the decomposition of a hydrocarbon gas in the presence of transition-metal catalyst particles, are an interesting type of carbon material that has been receiving considerable research attention since its development a few decades ago up to the present time [1–8]. The interest for CNFs arises from the combination of advantageous physical properties, e.g. high electrical and thermal conductivity or good mechanical strength [7], with the prospect of low-cost and/or versatile mass production, for example, through their synthesis at room temperature [9]. Potential applications for this type of carbon fiber include its use as mechanical reinforcement of polymer composites [10, 11], hydrogen-storage material [12, 13], catalyst support [14–18], or as an anode additive in Li-ion batteries [19].

In the context of some of these applications, high temperature annealing treatments, i.e. graphitization, of the CNFs appear as an attractive means of finely controlling their structure and properties. The graphitization of CNFs has been studied in the past mainly by such techniques as X-ray diffraction (XRD), Raman spectroscopy, and scanning and transmission electron microscopy (SEM/TEM) [20–22]. However, the mentioned techniques do not allow a direct atomic-scale visualization of the structural changes induced by heat treatment. This type of atomic-scale information, considered helpful to gain a deeper understanding of the graphitization behavior of carbon materials and not available at present for CNFs, is best provided by some scanning probe microscopy (SPM) methods, especially scanning tunneling microscopy (STM) [23–25]. The other widely employed SPM variant, namely atomic force microscopy (AFM), is less suitable for this purpose, as it lacks sufficient resolution to image defects and disordered structures at the atomic level, which STM can readily unveil [24, 26–28]. As a matter of fact, STM has recently proven useful for the atomic-scale characterization of pristine and plasma-treated CNFs [29, 30]. Nonetheless, it should be noted that AFM can be employed to reveal general lattice periodicities on ordered surfaces [26], and in this respect some research has already been carried out with graphitized fibers [31].

Here, the graphitization process of CNFs (~ 100 nm in diameter) is investigated on a local (nanometric and atomic) scale by means of STM. For this purpose, the structural changes of samples heat treated at different temperatures are analyzed. To complement the local information obtained by STM, the results of a global structural characterization by XRD and Raman spectroscopy are also presented. CNFs have been chosen in this study mainly for two reasons: (i) they are of particular interest in their graphitized state for some applications, for example as a filler to improve the performance of Li-ion batteries [19] or electrically conducting polymer composites [32]; and (ii) from a fundamental carbon-science perspec-

✉ Fax: +49-711-689-1010, E-mail: j.paredes@fkf.mpg.de

tive, they offer the opportunity to study in detail potentially new aspects in the graphitization of carbon materials confined to the nanometer scale.

2 Experimental

Pristine, as-produced CNFs, with typical diameters around 100 nm, were obtained from Applied Sciences, Inc. (Cedarville, OH, USA) and used as starting material. A detailed account of their production process and basic structural characteristics has been given previously [33, 34]. Heat treatment of the nanofibers was carried out at three different temperatures (1800, 2300, and 2800 °C) in a graphite-resistance furnace operating under a high-purity argon atmosphere. The samples were heated from ambient temperature to 1100 °C at a rate of 20 °C/min and from 1100 °C to the desired treatment temperature at 10 °C/min, and then maintained at such a temperature (monitored by an optical pyrometer) for 1 h, after which the furnace was turned off and the samples were allowed to cool in argon to room temperature.

XRD measurements of the different samples were performed on a Siemens D5000 powder diffractometer that uses Cu K_α radiation ($\lambda = 0.154056$ nm), at a step size and time of 0.015° (2θ) and 3 s, respectively. Peak broadening (0.1475°) was determined by means of a reference Si crystal. Raman spectra were recorded with a laser excitation wavelength of 632.8 nm on a Jobin–Yvon LabRam apparatus, covering a spectral range from 150 to 3900 cm^{-1}. To avoid sample damage due to local overheating by the laser, the incident laser power was set to 4 mW. The acquisition time for each spectrum was 400 s. STM investigations were accomplished with a Nanoscope Multimode IIIa, from Digital Instruments, in air at room temperature. A small quantity of pristine or heat-treated CNF sample was gently agglomerated into a pellet with the aid of a hydraulic press, mounted on the STM sampler holder, and imaged without further preparation. All the images were obtained in the constant-current mode (variable height) using mechanically prepared Pt/Ir (80/20) tips. Typical bias voltages and tunneling currents employed were 0.1–1.0 V and 0.4–1.0 nA, respectively, for non-

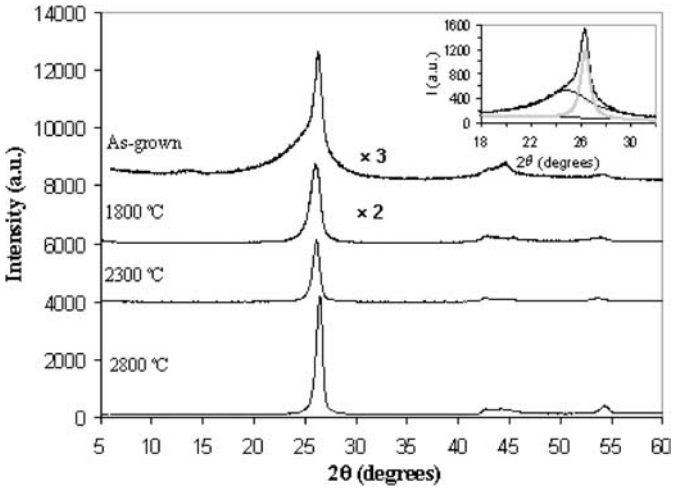

FIGURE 1 X-ray diffraction profiles of the as-grown and heat-treated CNF samples. *Top right inset*: deconvolution of the (002) peak for the as-grown sample

atomic scale imaging, and 10–100 mV and 1–8 nA, respectively, when imaging at the atomic scale. To check for the reproducibility of the STM observations and rule out possible artifacts in the images, several different and previously unused tips were employed. For every sample, a few hundred atomic-scale images were recorded on many different areas to ensure that the results were representative of the structural changes undergone by the nanofibers upon the annealing treatments.

3 Results and discussion

3.1 *Global structural characterization by XRD and Raman spectroscopy*

X-ray diffractograms for the as-grown and heat-treated CNF samples are presented in Fig. 1. As expected, the most visible feature is the graphite (002) diffraction line, located at $\sim 26°$. Also discernible are the (100) and (101) reflections, which appear in the region between 42 and 45° forming a broad band, and the (004) line near 55°. We note that the (002) peak narrows and increases in intensity with increasing heat-treatment temperature, and a similar trend is observed for the other lines, which indicates a general development of both intra- and interplane graphitic order. Likewise, it is apparent that the (002) peak of the as-grown sample has a broad shoulder on its low-angle side. Indeed, the peak can be deconvoluted [34] (inset at the top right corner of Fig. 1) to yield a sharp line centered at about 26.3°, characteristic of an ordered graphitic phase, and a broad band at 24.7°, indicative of only partially ordered carbon. Considering the known duplex structure of this carbon nanofiber [34], the ordered phase can be ascribed to the graphitic inner filament and the less ordered phase to the relatively amorphous carbon outer layer. Table 1 lists some crystallographic parameters deduced for the two phases: the interlayer spacing (d_{002}) and the apparent crystallite size along the c axis (L_c). L_c was calculated using Scherrer's formula. Upon heat treatments of increasing temperature, the (002) peak becomes more symmetric as the shoulder tends to disappear (Fig. 1), reflecting the gradual

Sample	Disordered		Graphitic		
	$d_{(002)}$	L_c	$d_{(002)}$	L_c	R
As-grown	0.357	1.7	0.339	9.6	0.60
1800 °C	0.345	6.9	0.339	11.0	1.10
2300 °C	0.341	10.9	0.339	11.0	5.96
2800 °C	0.339	11.0	0.336	19.5	11.95

TABLE 1 Interlayer spacing $d_{(002)}$, apparent crystallite size L_c along the c axis, both in nm, for the disordered and graphitic phases of the CNFs, and ratio of graphitic and disordered areas, R, as deduced from XRD data

conversion of the disordered phase into graphitic carbon. However, some degree of asymmetry is retained even for the sample graphitized at 2800 °C, implying that structural disorder has prevailed to a certain extent. Although in the case of the heat-treated samples the distinction between the two originally segregated phases (i.e. crystalline and amorphous) becomes blurred, their (002) peaks were also deconvoluted and their relative areas and corresponding crystallographic parameters calculated (Table 1), in order to quantitatively assess the extent of graphitization. From Table 1, we see that the area ratio graphitic/disordered (R) increases with temperature, as expected. Also, the interlayer spacing d_{002} and the apparent crystallite size L_c are seen to steadily decrease and increase, respectively, with heat-treatment temperature, which indicates an enhancement of graphitic ordering. At the highest temperature (2800 °C) the d_{002} values are very close, although not coincident, to that of perfect graphite (0.335 nm), suggesting a highly graphitic final material with some remaining structural defects.

Figure 2 shows the first-order (1000–1900 cm^{-1}) and second-order (2300–3300 cm^{-1}) Raman spectra of the as-grown and heat-treated nanofiber samples. The first-order spectra display two main bands: the D band, which is disorder-induced and not present in highly ordered graphites, at about 1335 cm^{-1}, and the G (graphite mode) band at $\sim$ 1580 cm^{-1}. A smaller peak at 1620 cm^{-1}, the D' band, particularly apparent for the heat-treated samples, is observed as well. The line widths of all these bands decrease with increasing graphitization temperature, indicating the progressive removal of structural disorder by the annealing process [35]. Another indicator of the development of graphitic order is the ratio between the integrated intensities of the D and G bands, I_D/I_G. This ratio, shown in Fig. 2 for each spectrum, diminishes dramatically with increasing heat-treatment temperature. However, it retains a non-negligible value even for the highest temperature, i.e. the D band does not completely disappear, indicating that some degree of structural disorder is kept upon graphitization. This observation is consistent with the XRD results and with previous Raman measurements reported for similar fibers [20]. In the second-order spectra (Fig. 2), the most prominent feature is a band at $\sim$ 2660 cm^{-1} that is broad and weak for the as-grown sample and becomes sharper and more intense for the heat-treated nanofibers. This band corresponds to the second harmonic of the D line, and in the present case maintains a symmetric shape throughout the heat treatments, implying that full removal of defects, especially those affecting the long-range three-dimensional ordering, is not achieved [35]. The incomplete three-dimensional ordering upon heat treatment is attributed to the spatial constraints imposed on graphitization by the small diameter of the fibers. Concerning the other bands in the second-order spectra, these are much weaker and include a disorder-induced line at around 2930 cm^{-1}, which decreases with increasing temperature, and the second harmonic of the D' line at 3240 cm^{-1}.

In addition, we should note that a distinct peak was observed in the low-frequency region of the Raman spectra, as exemplified in the top right inset of Fig. 2 for the sample heat treated at 2800 °C. The peak is located at $\sim$

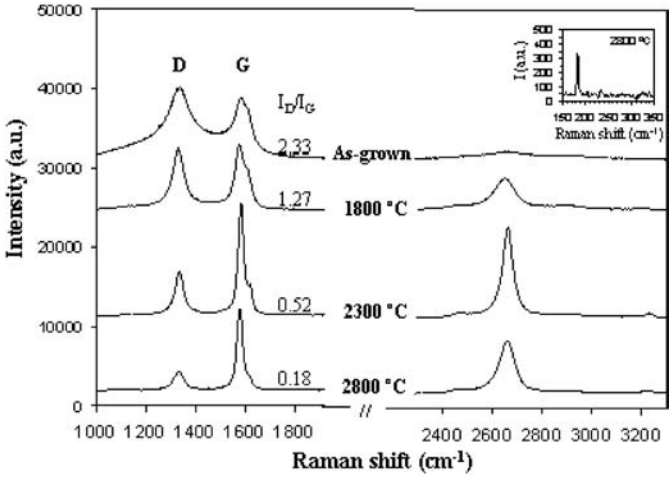

FIGURE 2 First- and second-order Raman spectra of the as-grown and heat-treated CNF samples. *Top right inset*: low-frequency region of Raman spectrum for the sample heat treated at 2800 °C

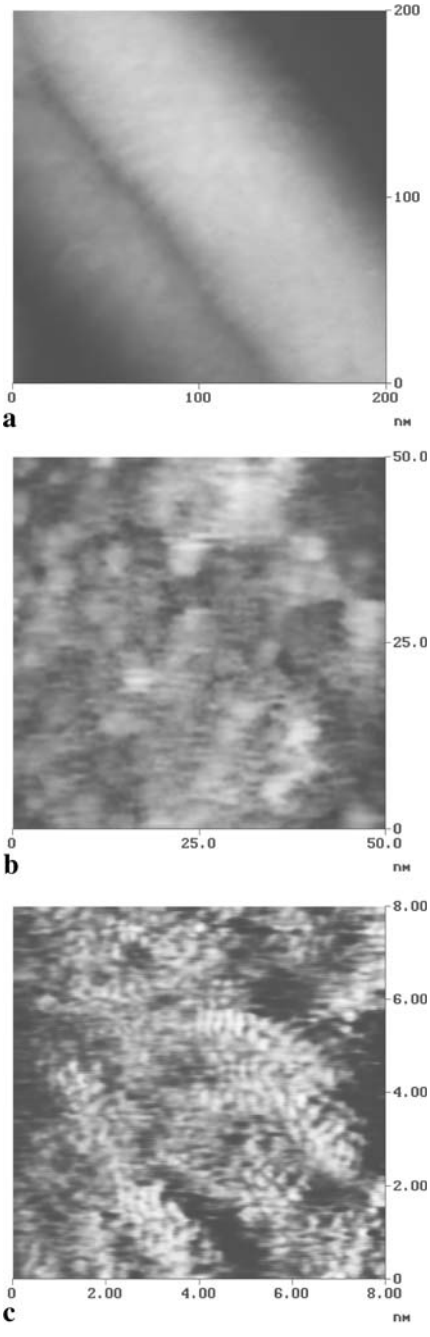

FIGURE 3 Representative STM images of the as-grown CNF sample. **a** General view of two nanofibers. **b** Nanometer-scale structure of an individual nanofiber. **c** Atomic-scale structure

$182\,\mathrm{cm}^{-1}$ and appeared consistently at the same position for all samples (starting as well as heat-treated at all temperatures), albeit in all cases its intensity was very small compared to the G or D bands. For carbon materials, low-frequency Raman modes with frequencies similar to the one reported here arise from the radial breathing vibrations of rolled-up graphenes of very small diameter ($\lesssim 2\,\mathrm{nm}$), i.e. they originate from single-walled carbon nanotubes (SWNTs) [36, 37] or from very thin innermost tubes of multiwalled nanotubes (MWNTs) [38–40]. Another possibility could be the presence of carbon nano-onions, but in this instance strong additional peaks should also be observed at intermediate frequencies (500–$1200\,\mathrm{cm}^{-1}$) [41], which was not the case for the present samples. Therefore, the peak at $\sim 182\,\mathrm{cm}^{-1}$ is attributed to the presence of SWNTs or MWNTs that have formed during the nanofiber-production process. Indeed, previous TEM studies have revealed that a small fraction of carbon nanotubes, essentially of multiwall type, can be adventitiously produced during the synthesis of carbon fibers and nanofibers by the same procedure as that employed for the nanofibers investigated here [42, 43]. As we will see below, the STM observations also suggest the presence of MWNTs in our samples.

3.2 *Local structural characterization by STM*

Figure 3 shows representative STM images of the as-grown CNFs at three different magnifications. Since an in-depth description of the pristine, as-produced nanofibers by STM has been given elsewhere [29], only their main characteristics will be outlined here, especially those relevant to understand the structural evolution of the material upon heat treatment. In a general view displaying two nanofibers (Fig. 3a), it is verified that they have diameters of the order of 100 nm. At this scale, the nanofibers exhibit a very smooth morphology without any particularly significant features. Also, height profiles taken along directions perpendicular to the axis of the nanofibers (not shown) clearly revealed their curved, i.e. cylindrical, geometry. The nanometer-scale structure of the material was disclosed upon detailed inspection of individual nanofibers (Fig. 3b). It is seen that the surface comprises tiny platelets with more or less rounded shapes, diameters typically between 1.5 and 5 nm, and heights equivalent to those of a few ($\sim$ 2–4) graphenes. The platelet arrangement is isotropic, i.e. there is no specific orientation of the features in any direction, e.g. parallel or perpendicular to the nanofiber axis. On the atomic scale (Fig. 3c), an absence of long-range graphitic order is evident and only structured areas of very small size ($\lesssim 2\,\mathrm{nm}$) can be identified. Likewise, the atomic-sized spots within the structured areas form arrays that are just vaguely ordered and different to the perfect triangular pattern commonly observed by STM on highly ordered graphites [28]. Furthermore, although the spot-to-spot distances in these arrays are around 0.25 nm, which corresponds to the periodicity of the STM pattern

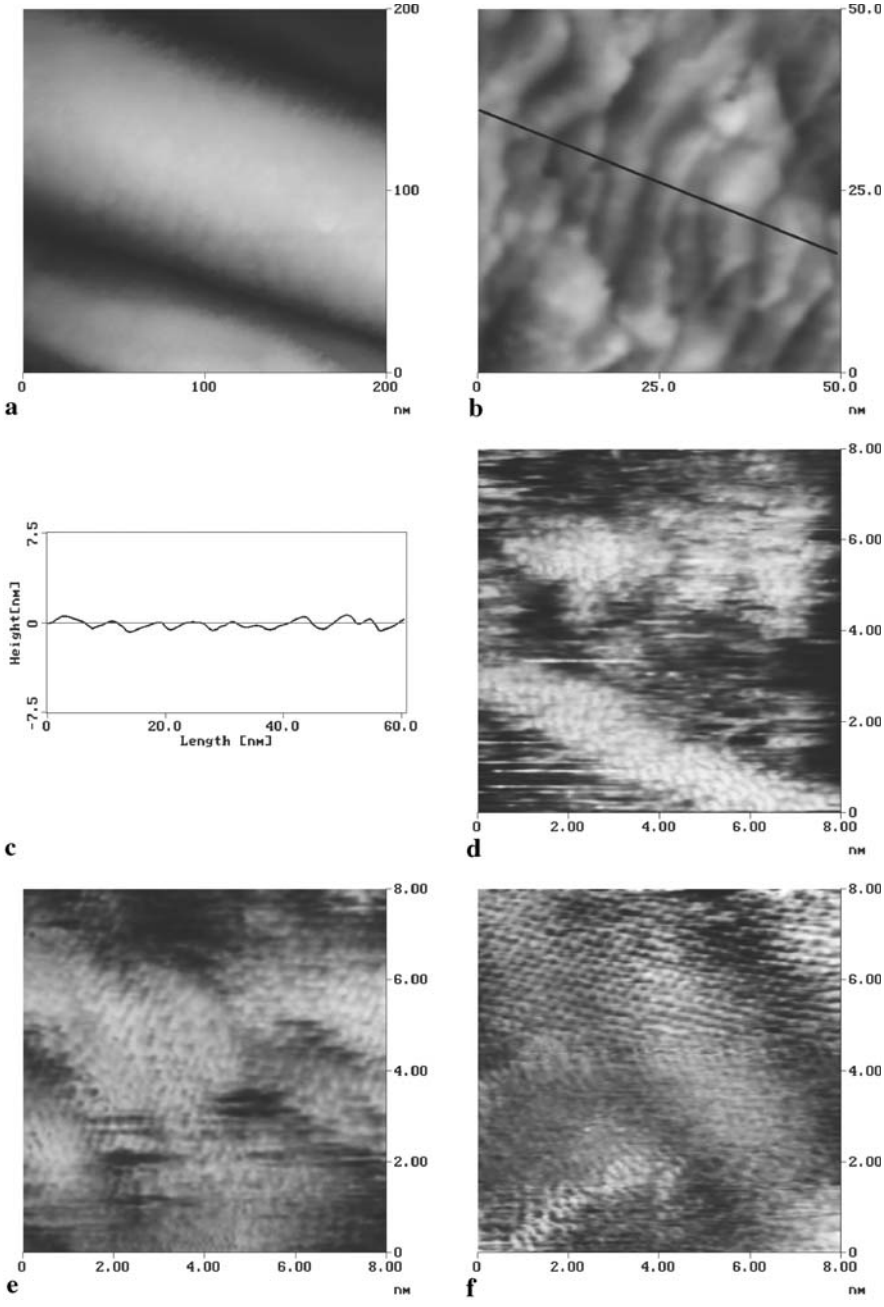

FIGURE 4 STM images of CNF sample heat treated at 1800 °C. **a** General view. **b** Detailed structure on the nanometer scale. **c** Height profile taken along the *black line* direction in (**b**). **d–f** Atomic-scale structure

of perfect graphite, they exhibit considerable local variations. The small structured areas are interpreted as tiny crystallites (a few nm wide and a few graphenes thick) that constitute the basic structural unit of the nanofiber outer layer, and it is reasonable to assume that their evolution with heat treatment will determine the graphitization behavior of the material. The flawed internal disposition of these basic units, as detected by STM, can be attributed to perturbations induced by a number of factors: a large proportion of edge carbon atoms in the crystallite, a faulty stacking of the minute graphenes, or the presence of heteroatoms, interstitials, and atomic vacancies, all of which are known to perceptibly affect the atomic-scale structures probed by the technique [23, 28, 44–46]. Although in a different context, imperfect internal arrangements have also been observed in the STM images of polycyclic aromatic hydrocarbons (PAHs) deposited on a graphite substrate [47]. These PAH molecules can be regarded as model nanographenes and would thus constitute an idealized version of the basic units described here for the CNFs.

Upon heat treatment at 1800 °C, the CNFs were seen to undergo structural changes both at the nanometer and atomic scales. Typical STM results for this temperature are presented in Fig. 4. In low-magnification images (Fig. 4a), the nanofibers displayed again a very smooth overall appearance. Furthermore, line profiles revealed that the cylindrical geometry characteristic of the as-grown nanofibers was preserved during the heat treatment. However, even at the resolution level of Fig. 4a, the fine texture looked somewhat different to that of the starting material (Fig. 3a). This was confirmed when individual nanofibers were examined at higher resolution, as exemplified in Fig. 4b. Now, the fiber nanostructure is dominated by an approximately striped morphology. The stripes are quite irregular in contour, rather than being perfectly straight, and their widths range from about 3 to 8 nm. It can also be noticed that they are aligned more or less perpendicularly to the fiber axis, which is indicated by the black line in Fig. 4b. A height profile taken along this line (Fig. 4c) reveals a saw-toothed topography consisting of basically flat terraces, which correspond to the stripes, separated by steps. Measurement of step heights yielded values that were roughly an integer number (typically 1 to 4) times the interlayer spacing of graphite (0.335 nm). All these observations strongly suggest that the transition from a platelet morphology (as-grown nanofiber, Fig. 3b) to a striped structure (nanofiber heat treated at 1800 °C, Fig. 4b) proceeds through coalescence of the tiny crystallites characteristic of the original nanofiber into larger units. This is supported by the atomic-scale images of the heat-treated samples (Fig. 4d–f). Again, in this case, structured areas lacking the perfect STM triangular pattern of highly ordered graphites were usually observed. Nevertheless, their size increased noticeably, reaching average lateral dimensions of 3–4 nm. For instance, in Fig. 4d a long (> 8 nm), thin (∼ 2 nm) atomically resolved domain is noticed in the bottom half of the image. As such long structured areas were never observed in the

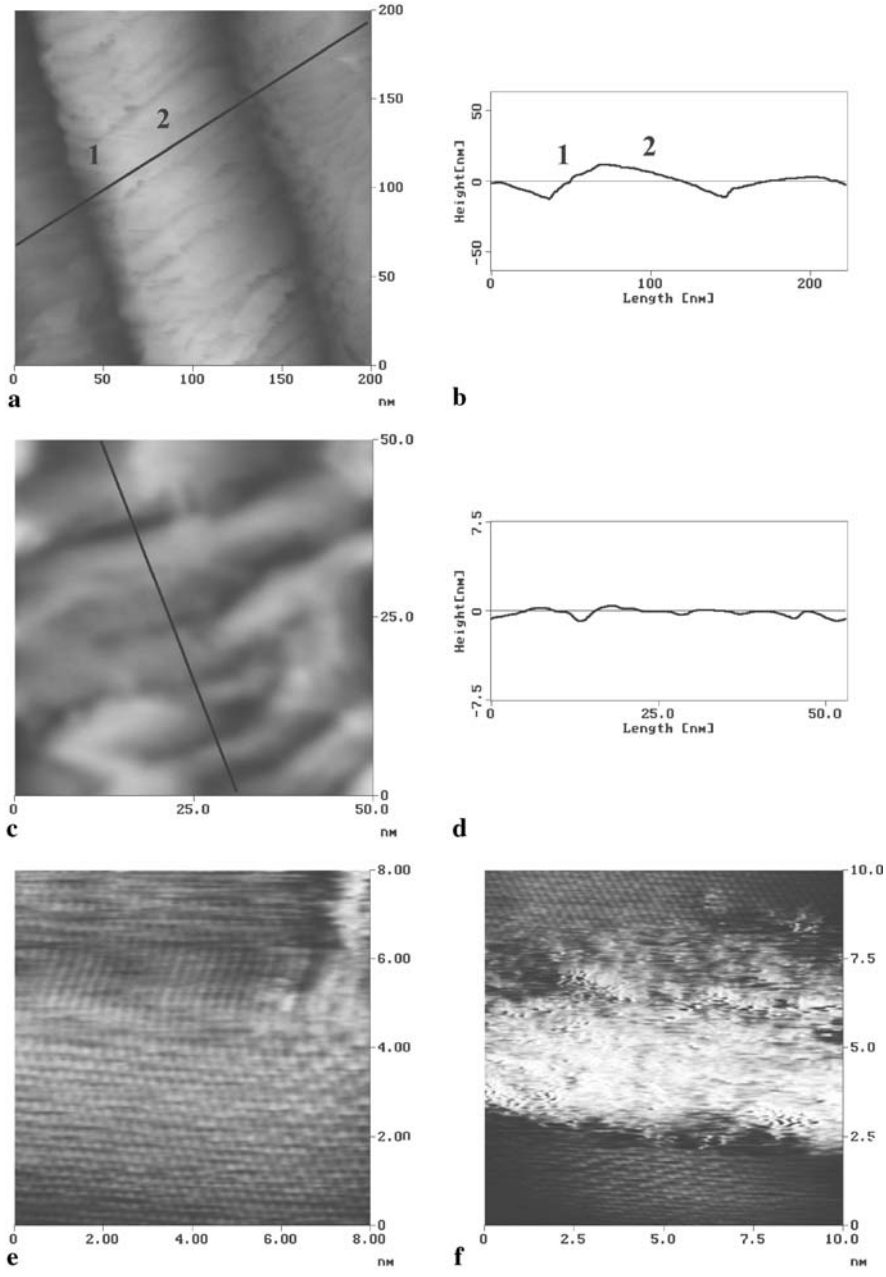

FIGURE 5 STM images of CNF sample heat treated at 2300 °C. **a** General view. **b** Height profile taken along the *black line* direction in (**a**). **c** Nanometric structure of an individual nanofiber. **d** Height profile taken along the *black line* direction in (**c**). **e**, **f** Atomic-scale structure

original nanofibers, we conclude that they develop upon the annealing treatment. In addition to this long domain, we notice in Fig. 4d another relatively large structured area located in the top part of the image. By contrast, the region in between appears unresolved on the atomic scale, indicating that a high degree of disorder is still retained in some sections of the heat-treated nanofibers. In other parts of the nanofibers, however, the now enlarged structured domains are more compactly arranged, as seen in Fig. 4e, and are separated just by discontinuities in the disposition of the atomic-sized spots, rather than by atomically unresolved sections. Although the dominant features in the atomic-scale images of the 1800 °C sample were those illustrated in Fig. 4d and e, we should note that, in a few cases, and in limited areas, a higher degree of order could be observed. An example is presented in Fig. 4f, where the triangular pattern with a periodicity of 0.25 nm archetypal of graphitic order is recognized. Overall, the STM results for this sample, which indicated a general albeit limited enhancement in the atomic-scale order of the nanofibers after heat treatment at 1800 °C, are consistent with the XRD and Raman data discussed previously. The coalescence of the tiny crystallites into larger units at this temperature can be explained by the release of hydrogen and heteroatoms (e.g. oxygen) that were originally bonded and provided stabilization to the crystallite edge carbon atoms [22, 29]. Thus, when the former are released, the latter have to be stabilized again by bonding to their counterparts at neighboring crystallites [22], which consequently merge and form larger units.

Further structural changes were observed when the heat-treatment temperature was increased to 2300 °C. Figure 5 shows some representative STM images for this temperature. The low-magnification images (Fig. 5a) reveal a general morphological transformation of the nanofibers, which is best evidenced in the height profile (Fig. 5b) taken along the black line of Fig. 5a. The nanofibers display an essentially faceted geometry, as opposed to the circular cross section of the as-grown and 1800 °C heat-treated nanofibers. The nanofiber shown in Fig. 5a exhibits two facets to the sample surface, marked as 1 and 2 in both the image and the height profile. The faceting phenomenon of this type of carbon fiber subjected to high-temperature heat treatment has been reported previously [2, 20], and is triggered by the release of strain energy during the transformation of a curved graphene into a flat one. The detailed nanostructure of the facets is presented in Fig. 5c. Again, a striped arrangement more or less perpendicular to the fiber axis (black line) is observed, but in this case the stripes tend to be wider (∼ 6–12 nm) than those of the sample heat treated at 1800 °C. A typical height profile, taken along the black line direction, is given in Fig. 5d, where the wide stripes are clearly evident. On the atomic scale, the most prominent change at this temperature was the overall development of a genuinely graphitic order, i.e. the appearance of the well-known STM triangular pattern with a periodicity of 0.25 nm on

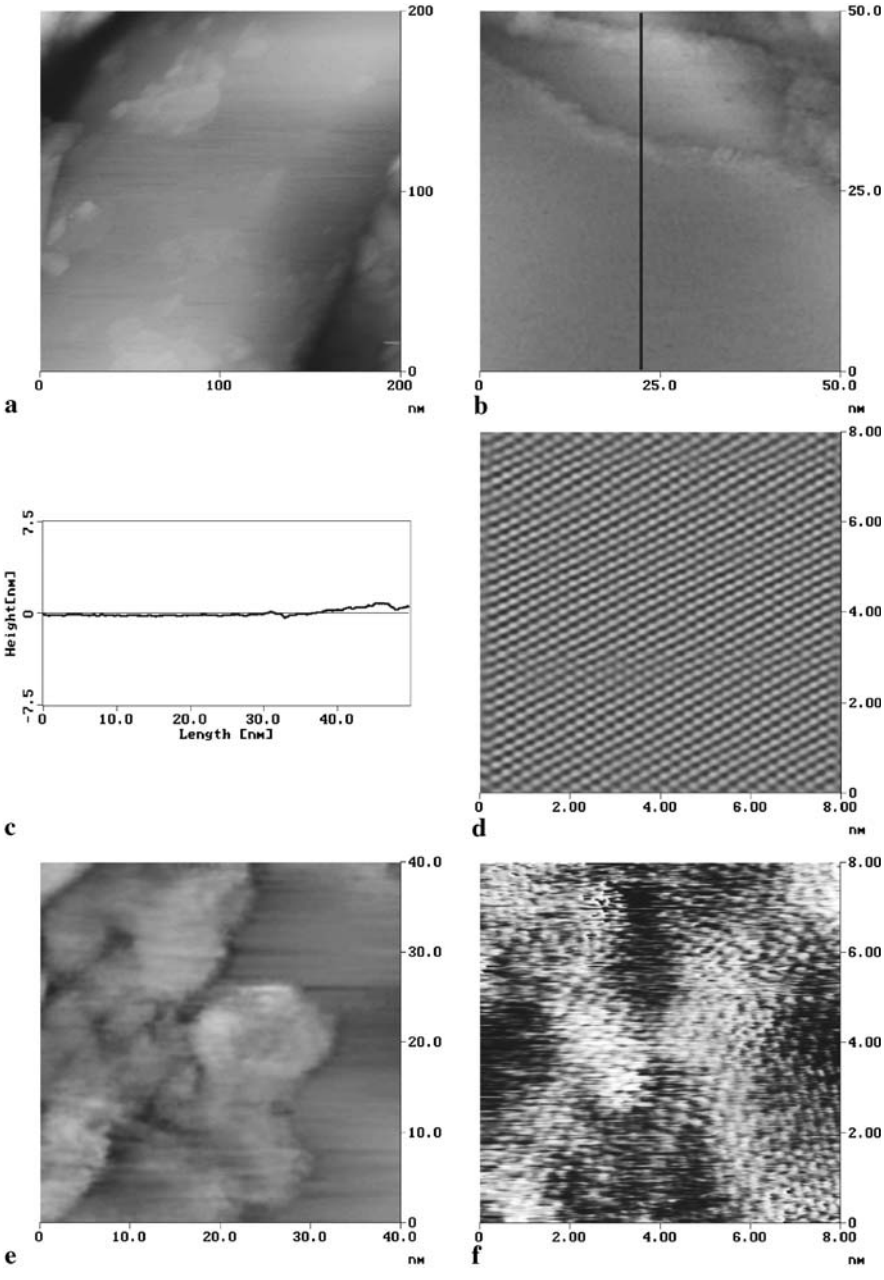

FIGURE 6 STM images of CNF sample heat treated at 2800 °C. **a** General view of a single nanofiber. **b** Terraced structure typical of nanofibers annealed at this temperature. **c** Height profile taken along the *black line* direction in (**b**). **d** Atomic-scale structure seen on the terraces. **e** Patches occasionally found on the terraces. **f** Atomic-scale structure of the patches

many locations. Nevertheless, many imperfections are still observable in the nanofiber structure, as exemplified in Fig. 5e and f. In Fig. 5e, the perfect graphitic structure in the bottom half of the image is interrupted by a discontinuity and a somewhat defective arrangement in the upper part. In Fig. 5f, we see a bright ($\sim$ 0.5-nm high), disordered region about 3-nm wide in between two perfectly graphitic areas. This type of large, disordered feature was never observed in the other samples, and might seem contradictory with the general enhancement of crystalline order described for this temperature, as revealed not only by STM but also by XRD and Raman spectroscopy. A plausible explanation for this observation would be the following: at around 2000 °C, point defects such as atomic vacancies are known to become mobile in graphitizable carbons [24]. Such mobility would lead to the release of the point defects from many areas, which would thus develop a highly graphitic structure, as is indeed reported for the present sample. However, it is also reasonable to assume that in their migration, the atomic vacancies can also aggregate in some areas, forming relatively large clusters of vacancies [48, 49]. Taking into account that the latter type of defect appears in the STM images of graphite as bright, disordered regions with dimensions of several nm [28, 45], we argue that the bright feature of Fig. 5f could correspond to an area where the mobile atomic vacancies have accumulated.

Figure 6 presents the STM results obtained for a heat-treatment temperature of 2800 °C. In this sample, the nanofibers exhibited very well developed facets, as shown in Fig. 6a. The facets were essentially featureless, except for the occasional presence of some patches. The areas outside the patches consisted of atomically flat terraces up to several tens of nm wide, separated by steps (see Fig. 6b and corresponding height profile in Fig. 6c), similarly to what has been observed in highly ordered graphites. Atomic-scale imaging on the terraces (Fig. 6d) corroborated the presence of long-range graphitic order at this temperature. A detailed image of the patches, which we interpret as remnant fragments of graphenes from the graphitization process, is provided in Fig. 6e. They appear as smooth, more or less rounded domains several nm in diameter, and their height corresponds to that of one to three graphenes lying over the atomically flat terraces. On the atomic scale (Fig. 6f), we notice the coexistence in the patches of perfect graphitic structures (e.g. bottom right corner of the image) with superstructures of $\left(\sqrt{3}\times\sqrt{3}\right)R30^\circ$ type (center of the image). This type of superstructure is frequently observed by STM around defects or discontinuities in otherwise highly ordered graphites [24, 28, 45, 46, 49], and has been attributed to a local modulation of the electronic density near the Fermi level induced by the defect or discontinuity. The presence of such defective structures on the graphitized nanofiber surface, together with the structural imperfections that we assume to exist beneath the surface at the junctions between different facets, should contribute to the non-negligible D band in the Raman spectra that is retained after heat treatment even at this high temperature (Fig. 2).

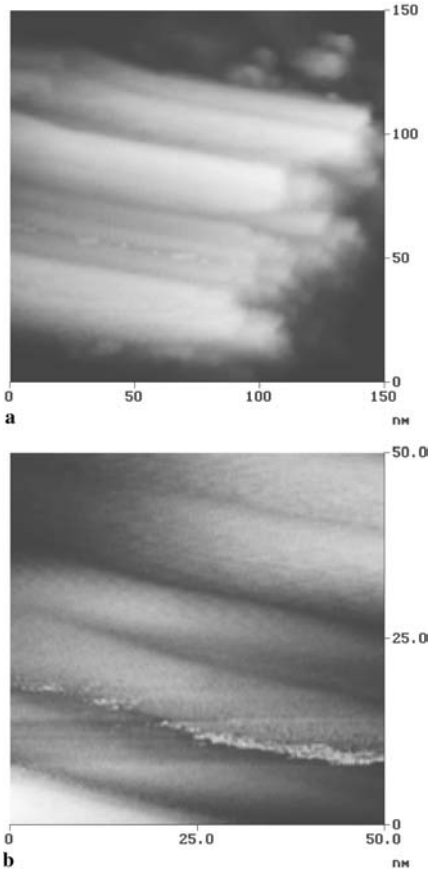

FIGURE 7 STM images of rod-like features observed on the CNF samples and attributed to MWNTs. **a** General view. **b** Enlarged image

Finally, we should mention that in a few occasions we observed some features in the STM images that could not be attributed to the CNFs. An example is shown in Fig. 7, taken from the 2800 °C sample. In Fig. 7a, the features seem to be a cluster of rods. Although the rods are reminiscent of the stripes described for the samples heat treated at 1800 and 2300 °C, they are not part of a nanofiber, as lower-magnification images indicated. A more detailed image (Fig. 7b) reveals that the rods, with typical diameters of $\sim$ 10 nm, have an extremely smooth surface. Since (i) this sort of structure is very similar to that observed by STM on carbon-nanotube bundles [50, 51], (ii) carbon nanotubes have been reported to be unintentionally grown in the production of this type of carbon fiber [42, 43], and (iii) the low-frequency Raman spectra of our samples (inset of Fig. 2) were also consistent with the presence of nanotubes, we tentatively ascribe the rods in Fig. 7 to multiwalled carbon nanotubes.

4 Conclusions

STM has proven useful to reveal, on a very local scale, the structural evolution of CNFs submitted to high-temperature heat treatments. Taken together, the STM images provided clear evidence of the gradual graphitization of the nanofibers and annealing of structural defects with increasing heat-treatment temperature, consistent with the results obtained from global characterization techniques, namely, XRD and Raman spectroscopy. More specifically, at the nanometer scale STM revealed a transformation from a platelet morphology to one consisting of increasingly wider stripes, and finally to a structure of atomically flat terraces on faceted nanofibers. These changes chimed in with those observed at the atomic scale: the minute, highly defective crystallites characteristic of the starting nanofiber coalesced upon heat treatment at 1800 °C to form larger although still defective crystallites. A large number of defects were annealed out at 2300 °C, leading to the development of truly graphitic domains on many areas, as evidenced by the appearance of the well-known STM triangular pattern with a periodicity of 0.25 nm. However, highly disordered sections were

also generated at this temperature and attributed to the aggregation of mobile point defects (atomic vacancies). Such defects disappeared from the nanofibers heat treated at 2800 °C, which displayed large crystalline areas, exhibiting a low coverage of small fragments of incompletely graphitized graphenes.

ACKNOWLEDGEMENTS Financial support from the 3rd PRI Asturias (Project No. PB02-96) is gratefully acknowledged. J.I. Paredes also acknowledges a postdoctoral fellowship from the Ministerio de Educación, Cultura y Deporte, Spain.

REFERENCES

1 R.T.K. Baker, M.A. Barber, R.J. Waite, P.S. Harris, F.S. Feates: J. Catal. **26**, 51 (1972)
2 R.T.K. Baker, P.S. Harris, R.B. Thomas, R.J. Waite: J. Catal. **30**, 86 (1973)
3 R.T.K. Baker, P.S. Harris, S. Terry: Nature **253**, 37 (1975)
4 R.T.K. Baker, R.J. Waite: J. Catal. **37**, 101 (1975)
5 M. Audier, J. Guinot, M. Coulon, L. Bonnetain: Carbon **19**, 99 (1981)
6 M. Audier, A. Oberlin, M. Oberlin, M. Coulon, L. Bonnetain: Carbon **19**, 217 (1981)
7 L.P. Biró, C.A. Bernardo, G.G. Tibbetts, P. Lambin (Eds.): *Carbon Filaments and Nanotubes: Common Origins, Differing Applications?* (Kluwer, Dordrecht 2001)
8 S. Helveg, C. López-Cartes, J. Sehested, P.L. Hansen, B.S. Clausen, J.R. Rostrup-Nielsen, F. Abild-Pedersen, J.K. Nørskov: Nature **427**, 426 (2004)
9 B.O. Boskovic, V. Stolojan, R.U.A. Khan, S. Haq, S.R.P. Silva: Nat. Mater. **1**, 165 (2002)
10 S. Kumar, H. Doshi, M. Srinivasarao, J.O. Park, D.A. Schiraldi: Polymer **43**, 1701 (2002)
11 D. Shi, J. Lian, P. He, L.M. Wang, F. Xiao, L. Yang, M.J. Schulz, D.B. Mast: Appl. Phys. Lett. **83**, 5301 (2003)
12 D.J. Browning, M.L. Gerrard, J.B. Lakeman, I.M. Mellor, R.J. Mortimer, M.C. Turpin: Nano Lett. **2**, 201 (2002)
13 A.D. Lueking, R.T. Yang, N.M. Rodriguez, R.T.K. Baker: Langmuir **20**, 714 (2004)
14 N.M. Rodriguez, M.-S. Kim, R.T.K. Baker: J. Phys. Chem. **98**, 13 108 (1994)
15 T.G. Ros, A.J. van Dillen, J.W. Geus, D.C. Koningsberger: Chem. Eur. J. **8**, 2868 (2002)
16 T.G. Ros, D.E. Keller, A.J. van Dillen, J.W. Geus, D.C. Koningsberger: J. Catal. **211**, 85 (2002)
17 E.S. Steigerwalt, G.A. Deluga, C.M. Lukehart: J. Phys. Chem. B **106**, 760 (2002)
18 R. Vieira, C. Pham-Huu, N. Keller, M.J. Ledoux: Chem. Commun. 954 (2002)
19 S.-H. Yoon, C.-W. Park, H. Yang, Y. Korai, I. Mochida, R.T.K. Baker, N.M. Rodriguez: Carbon **42**, 21 (2004)
20 M. Endo, K. Nishimura, Y.A. Kim, K. Hakamada, T. Matushita, M.S. Dresselhaus, G. Dresselhaus: J. Mater. Res. **14**, 4474 (1999)
21 G.-B. Zheng, H. Sano, Y. Uchiyama: Carbon **41**, 853 (2003)
22 M. Endo, Y.A. Kim, T. Hayashi, T. Yanagisawa, H. Muramatsu, M. Ezaka, H. Terrones, M. Terrones, M.S. Dresselhaus: Carbon **41**, 1941 (2003)
23 H. Saadaoui, J.C. Roux, S. Flandrois, B. Nysten: Carbon **31**, 481 (1993)
24 B. Nysten, J.-C. Roux, S. Flandrois, C. Daulan, H. Saadaoui: Phys. Rev. B **48**, 12 527 (1993)
25 H.N. Lei, A. Métrot, M. Troyon: Carbon **32**, 79 (1994)
26 S.N. Magonov, M.-H. Whangbo: *Surface Analysis with STM and AFM* (VCH, Weinheim 1996)
27 J.R. Hahn, H. Kang, S. Song, I.C. Jeon: Phys. Rev. B **53**, R1725 (1996)
28 J.I. Paredes, A. Martínez-Alonso, J.M.D. Tascón: Langmuir **18**, 4314 (2002)
29 J.I. Paredes, A. Martínez-Alonso, J.M.D. Tascón: Carbon **39**, 1575 (2001)
30 J.I. Paredes, A. Martínez-Alonso, J.M.D. Tascón: Carbon **40**, 1101 (2002)
31 Y.A. Kim, T. Matusita, T. Hayashi, M. Endo, M.S. Dresselhaus: Carbon **39**, 1747 (2001)
32 I.C. Finegan, G.G. Tibbetts: J. Mater. Res. **16**, 1668 (2001)
33 G.G. Tibbetts, D.W. Gorkiewicz, R.L. Alig: Carbon **31**, 809 (1993)
34 G.G. Tibbetts, G.L. Doll, D.W. Gorkiewicz, J.J. Moleski, T.A. Perry, C.J. Dasch, M.J. Balogh: Carbon **31**, 1039 (1993)
35 T.C. Chieu, M.S. Dresselhaus, M. Endo: Phys. Rev. B **26**, 5867 (1982)
36 A.M. Rao, E. Richter, S. Bandow, B. Chase, P.C. Eklund, K.A. Williams, S. Fang, K.R. Subbaswamy, M. Menon, A. Thess, R.E. Smalley, G. Dresselhaus, M.S. Dresselhaus: Science **275**, 187 (1997)
37 M.S. Dresselhaus, G. Dresselhaus, A. Jorio, A.G. Souza Filho, M.A. Pimenta, R. Saito: Acc. Chem. Res. **35**, 1070 (2002)
38 H. Jantoljak, J.-P. Salvetat, L. Forró, C. Thomsen: Appl. Phys. A **67**, 113 (1998)
39 X. Zhao, Y. Ando, L.-C. Qin, H. Kataura, Y. Maniwa, R. Saito: Chem. Phys. Lett. **361**, 169 (2002)
40 J.M. Benoit, J.P. Buisson, O. Chauvet, C. Godon, S. Lefrant: Phys. Rev. B **66**, 073 417 (2002)
41 D. Roy, M. Chhowalla, H. Wang, N. Sano, I. Alexandrou, T.W. Clyne, G.A.J. Amaratunga: Chem. Phys. Lett. **373**, 52 (2003)
42 M. Endo, K. Takeuchi, K. Kobori, K. Takahashi, H.W. Kroto, A. Sarkar: Carbon **33**, 873 (1995)
43 N. Jiang, R. Koie, T. Inaoka, Y. Shintani, K. Nishimura, A. Hiraki: Appl. Phys. Lett. **81**, 526 (2002)
44 H. Chang, A.J. Bard: J. Am. Chem. Soc. **113**, 5588 (1991)
45 J.R. Hahn, H. Kang: Phys. Rev. B **60**, 6007 (1999)
46 P.L. Giunta, S.P. Kelty: J. Chem. Phys. **114**, 1807 (2001)
47 P. Samorí, N. Severin, C.D. Simpson, K. Müllen, J.P. Rabe: J. Am. Chem. Soc. **124**, 9454 (2002)
48 K.H. Lee, H.M. Lee, H.M. Eun, W.R. Lee, S. Kim, D. Kim: Surf. Sci. **321**, 267 (1994)
49 B. An, S. Fukuyama, K. Yokogawa, M. Yoshimura: J. Appl. Phys. **92**, 2317 (2002)
50 K. Sattler: Carbon **33**, 915 (1995)
51 J.I. Paredes, F. Suárez-García, S. Villar-Rodil, A. Martínez-Alonso, J.M.D. Tascón, E.J. Bottani: J. Phys. Chem. B **107**, 8905 (2003)